

Review

All Inorganic Lead-Free Zero-Dimensional Metal Halide Luminescent Materials and Applications

Kashyap Dave , Wen-Tse Huang  and Ru-Shi Liu * 

Department of Chemistry, National Taiwan University, Taipei 106, Taiwan

* Correspondence: rslu@ntu.edu.tw; Tel.: +886-2-3366-1169

Abstract: Recently, zero-dimensional luminescent material has attracted researchers because of its optical properties, which is a possible candidate to replace lead halide perovskite. This review focused on the recent development of tetrahedrally and octahedrally coordinated inorganic halide semiconductor luminescent materials. We discuss the synthesis methods and crystal structures of these materials in this review. The materials are categorized based on the valence of central metal cations (monovalent, divalent, and trivalent). Finally, we have summarized the applications of these luminescent materials, such as light-emitting diodes, ultrafast switching memories, photodetectors, and scintillators. This review article provides an overview of recent progress on zero-dimensional materials and their applications for further development in the future.

Keywords: zero-dimensional; lead-free luminescent material; inorganic; metal halide

1. Introduction

Lead halide (CsPbX_3) ($X = \text{Cl}, \text{Br}, \text{and I}$) perovskite draws the attention of researchers because of its attractive properties for optoelectronics applications such as solar cells, light-emitting diodes, photodetectors, and scintillators [1–5]. Although these materials are used for various applications, the presence of lead (Pb) is a source of concern for researchers because of its toxicity. Several countries restrict the use of heavy metals for electronic devices, including lead. These concerns encourage researchers to move towards lead-free technology for these optoelectronics. Tin ion (Sn^{2+}) is an ideal element to substitute for Pb^{2+} because it is in the same group in the periodic table. However, Sn^{2+} is unstable in the atmosphere and oxidizes into Sn^{4+} , which makes an unstable perovskite structure [6]. It was initially observed that double perovskites are replaceable but have broadband white light emission with UV light excitation [7,8]. Several research groups have focused on developing zero-dimensional inorganic materials ($\text{A}_h\text{B}_k\text{X}_l$), which are ideal to replace lead halide perovskite [9]. In $\text{A}_h\text{B}_k\text{X}_l$ -type compounds, A is the monovalent cations ($\text{K}^+, \text{Cs}^+, \text{and Rb}^+$); B can be in monovalent, divalent, or trivalent cations; X can be halides ($\text{Cl}^-, \text{Br}^-, \text{and I}^-$); and ($1 < h, k, l < 9$). The zero-dimensional structure has isolated tetrahedral [BX_4] (Figure 1a) or octahedral [BX_6] (Figure 1b) coordination units [9,10]. The dimension relates to the arrangement of the inorganic unit at the molecular level rather than the particle size [9]. These structures attract researchers because of the isolated polyhedral inorganic units and extraordinary optical properties [11].

Only a few review articles have been published on zero-dimensional perovskite. Wang et al. [10] discuss the luminescence mechanism in zero-dimensional lead halide Cs_4PbBr_6 . Zhou et al. [12] summarized the work on organic–inorganic zero-dimensional material and their application for optoelectronics. Li et al. [9] discussed the organic–inorganic hybrid as well as all inorganic zero-dimensional materials with different optoelectronics applications. Recently several research articles have been published on all inorganic zero-dimensional materials with synthesizing techniques and applications, which is the focus of this review.



Citation: Dave, K.; Huang, W.-T.; Liu, R.-S. All Inorganic Lead-Free Zero-Dimensional Metal Halide Luminescent Materials and Applications. *Crystals* **2023**, *13*, 499. <https://doi.org/10.3390/cryst13030499>

Academic Editors: Sławomir Kaczmarek and Tomasz Bodziony

Received: 15 February 2023

Revised: 4 March 2023

Accepted: 10 March 2023

Published: 14 March 2023



Copyright: © 2023 by the authors. Licensee MDPI, Basel, Switzerland. This article is an open access article distributed under the terms and conditions of the Creative Commons Attribution (CC BY) license (<https://creativecommons.org/licenses/by/4.0/>).

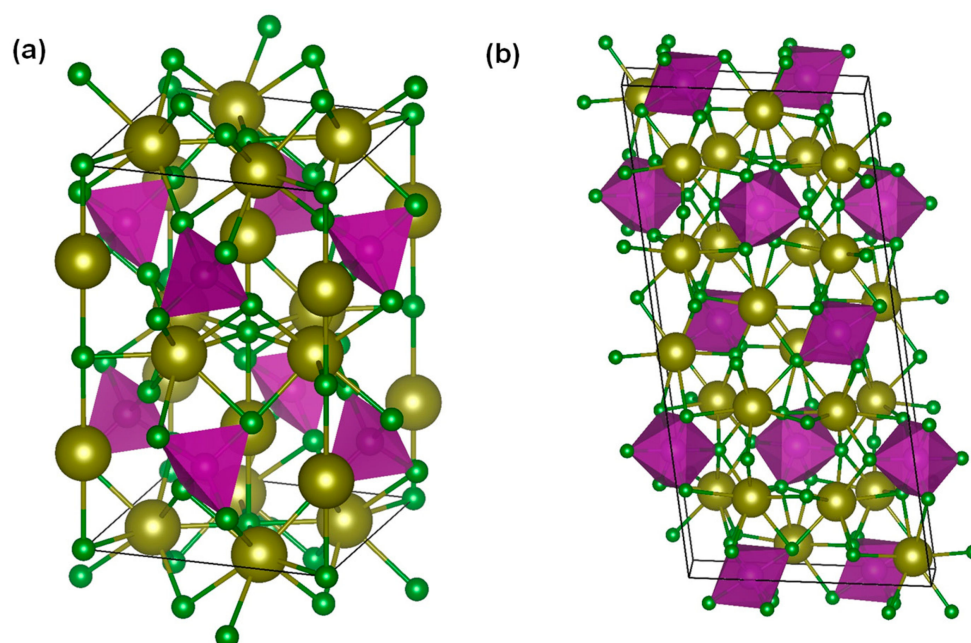


Figure 1. Crystal structure of electronically zero-dimensional with the isolated (a) tetrahedral and (b) octahedral.

In this review article, we have summarized recent development in tetrahedrally and octahedrally coordinated with all inorganic zero-dimensional material and their luminescent properties. We have deliberated the synthesis method, crystal structure, and luminescence properties. Finally, we have discussed the application of these materials for optoelectronics.

Luminescence Mechanism of Zero-Dimensional Metal Halide

Figure 2a illustrates the mechanism of light absorption and relaxation to emission lights Figure 2b–f. The photoluminescence mechanisms are categorized into intrinsic and extrinsic properties for solids. Intrinsic photoluminescence has band-to-band emission and exciton emission. In the band-to-band emission, the electron from the conduction band recombines with the valence band hole, shown in Figure 2b [13,14]. In exciton luminescence, photogenerated electron-holes attract each other, and the resulting recombination emits photons, as shown in Figure 2c [13]. On the other hand, for extrinsic luminescence, the impurities, doping ions, and defects make levels where electrons from the conduction band transfer and then relax to the ground level via radiative recombination, as shown in Figure 2d,e [14]. Additionally, in intrinsic and extrinsic photoluminescence, several alkali halides, metal halides, organic–inorganic halide crystals, and low-dimensional materials display a self-trap exciton (STE) emission [15]. The STE emission material has a large Stokes shift and broadband emission [7]. In this material, upon light illumination, the strong electron–phonon coupling between the excited electron and crystal lattice results in strong carrier–photon interactions, as shown in Figure 2f. In emission mechanisms, photogenerated electrons are trapped at different STE states to lower the energy, and holes also increase the energy [16]. Thus, the emitted energy lowers the excited energy in STE-derived emission [17]. These types of luminescence have been observed in halide-based soft lattices [18]. Most zero-dimensional materials also have STE emissions, which we discuss in the next section.

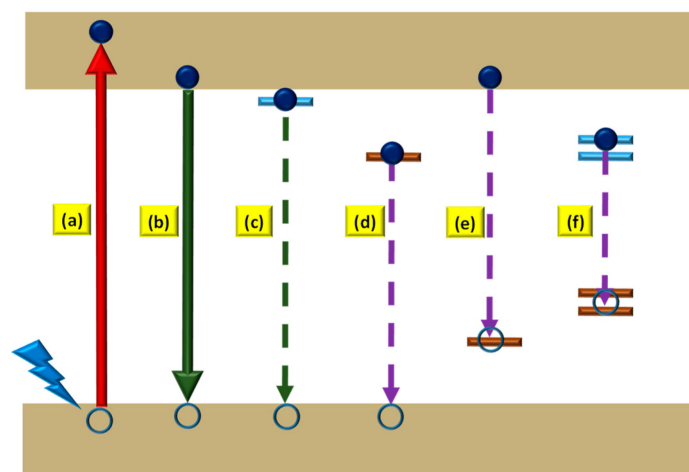


Figure 2. The possible emission mechanism for (a) light absorption, (b) band-to-band emission, (c) exciton emission, (d) emission from defects, (e) emission from ions, (f) self-trap exciton (STE) emission.

2. Zero-Dimensional Metal Halide Luminescent Materials

We have discussed in the introduction the general formula of compound ABX. This section discusses the coordination environment of B with monovalent, divalent, and trivalent coordination.

2.1. Mono-Valent Coordinated Zero-Dimensional Materials

2.1.1. Cu-Based

Copper-based CsCu_2I_3 , $\text{Cs}_3\text{Cu}_2\text{I}_5$, and $\text{Cs}_3\text{Cu}_2\text{Br}_{5-x}\text{I}_x$ are studied because of the high quantum yield for lighting and scintillation [19–22]. Liu et al. [19] used thermal evaporation to deposit $\text{Cs}_3\text{Cu}_2\text{I}_5$ for deep blue light emission at 440 nm. This method is suitable for making uniform and highly crystalline thin films. $\text{Cs}_3\text{Cu}_2\text{I}_5$ has an orthorhombic phase, with Cu^+ having two tetragonal and trigonal sites. The thermal evaporation was carried out using heating CsI and CuI above the melting point and deposited on a quartz/ITO substrate. The uniform thin film has a photoluminescence quantum yield of up to 58% [19]. In the past, several researchers reported using solution process synthesis nanocrystals first, followed by the deposition of these nanocrystals on the substrate. Wang et al. [20] synthesized $\text{Cs}_3\text{Cu}_2\text{I}_5$ nanocrystals by hot injection for blue light-emitting application. The crystal structure of $\text{Cs}_3\text{Cu}_2\text{I}_5$ has an orthorhombic phase, the same as thermal evaporated fabricated thin films. The photoluminescence quantum yield of this nanocrystal reached up to 87%, which is higher than the thin film and further applied for the blue LED [20]. Along with this, a solid-state reaction was used to synthesize $\text{Cs}_3\text{Cu}_2\text{I}_5$ bulk crystal with a quantum efficiency of up to 80% for white light emission on a 310 nm UV chip with green and red-emissive phosphors [23]. Roccanova et al. [21] used a solid solution to synthesize $\text{Cs}_3\text{Cu}_2\text{Br}_{5-x}\text{I}_x$ and achieved a PLQY of up to 98.7% for $\text{Cs}_3\text{Cu}_2\text{I}_5$. So far, all these studies have found that the bulk $\text{Cs}_3\text{Cu}_2\text{I}_5$ has high photoluminescence quantum yield compared to nanocrystals. $\text{Cs}_3\text{Cu}_2\text{I}_5$ is well synthesized for single crystals, nanocrystals, and microcrystals and used for blue light-emitting diodes and χ -ray imaging applications, which we discuss in the application sections.

2.1.2. Ag-Based

Ag-based compounds are reported with tunable emissions such as Cs_2AgCl_3 , Cs_2AgBr_3 , CsAgCl_2 , CsAgBr_2 , and Rb_2AgBr_3 [24,25]. Zhang et al. [24] used the ball milling method to synthesize bimetallic compound with tunable emission Cs-Ag-X ($x = \text{Cl}$ and Br). Cs_2AgX_3 has an orthorhombic crystal system with a $Pnma$ space group. These materials are excited with high energy photons and give emissions for Cs_2AgCl_3 , Cs_2AgBr_3 , CsAgCl_2 , and CsAgBr_2 at 397, 524, 620, and 820 nm, respectively. Resultantly these materials are unsuitable for WLED application and need further research to improve the issue. Defect-free

single crystals with this system can be used for X-ray scintillators with enhancing quantum yield. Toward the application of scintillation, Zhang et al. [25] synthesized a single crystal of Rb_2AgBr_3 . Rb_2AgBr_3 has broadband emissions centered at 468 nm. This system achieved a scintillation yield of up to 25,600 photons MeV^{-1} for χ -ray imaging. These results suggest the possible tunable emission with Ag-based compounds is attributed to a change in crystal structure and halides. We have added comparative photo-physical properties of 0D metal halide with monovalent units in Table 1.

Table 1. Properties of 0D metal halide with monovalent units.

Formula	Method	Isolated Species	Em. Wave. (nm)	FWHM (nm)	PLQY (%)	Ref.
$\text{Cs}_3\text{Cu}_2\text{I}_5$ Film	Thermal evaporation	$[\text{Cu}_2\text{I}_3]^-$	440	70	58	[19]
$\text{Cs}_3\text{Cu}_2\text{I}_5$ NC	Hot injection	$[\text{Cu}_2\text{I}_5]^{3-}$	445	63	87	[20]
Cs_2AgCl_3	Ball Milling	$[\text{AgCl}_4]^{3-}$	397	..	17	[24]
Cs_2AgBr_3	Ball Milling	$[\text{AgBr}_4]^{3-}$	524	..	21	[24]
Rb_2AgBr_3 SC	Cooling crystallization	$[\text{AgBr}_4]^{3-}$	488	..	27	[25]

2.2. Di-Valent Coordinated Zero-Dimensional Materials

2.2.1. Sn-Based

Tin ion (Sn^{2+}) is an ideal element to replace the lead ion (Pb^{2+}) in a three-dimensional APbX_3 perovskite system because they belong to the same group in the periodic table. However, Sn^{2+} is unstable and oxidizes into Sn^{4+} in moisture and water. Although several research groups have tried to make Sn-based three-dimensional perovskites, they are still not sufficiently stable for industrial applications. Recently several groups reported zero-dimensional Sn-based Cs_4SnX_6 ($\text{X} = \text{Cl}, \text{Br}, \text{and I}$) systems that can stabilize structures with Sn^{2+} for lighting applications. Both nanocrystal and bulk crystals are synthesized for Cs_4SnX_6 , which gives emission via the STE mechanism [26]. Cs_4SnBr_6 has a trigonal crystal system with the space group of $R\bar{3}c$, where $[\text{SnBr}_6]^{4-}$ is in isolated octahedral coordination [27]. Nanocrystals of Cs_4SnX_6 are synthesized by the hot-injection method in oleic acid and oleylamine in octadecene solvents. In the hot-injection method, Cs_2CO_3 and SnBr_2 precursors are dissolved in the nonpolar solvent 1-octadecene with ligands oleic acid and oleylamine at 120–150 °C in a vacuum separately. After that, Cs precursor is injected into Sn precursor in a nitrogen atmosphere at >160 °C. Further, the reaction is quenched by an ice or water bath to complete the formation of nanocrystals. Tan et al. [28] synthesized Cs_4SnBr_6 with partial and complete substitution with halide by the hot-injection method. The synthesized Cs_4SnBr_6 shows emission at 534 nm with an excitation wavelength of 365 nm. Partial substitution with iodide shifts emissions to 546 nm and complete substitution to 578 nm in $\text{Cs}_4\text{SnBr}_x\text{I}_{6-x}$, as shown in Figure 3a. Moreover, with substitutions, the PLQY for Cs_4SnBr_6 , $\text{Cs}_4\text{SnBr}_x\text{I}_{6-x}$, and Cs_4SnI_6 are 21%, 6.6%, and 0.7%, respectively. These three systems have a large Stokes shift with high FWHM, confirming the STE-derived emission. Xu et al. [29] modified the hot-injection method to improve luminescence properties, as shown in Figure 3b for Cs_4SnBr_6 , $\text{Cs}_4\text{SnBr}_3\text{I}_3$, and Cs_4SnI_6 . The synthesized Cs_4SnBr_6 compound has an emission at 537 nm with a PLQY of 52%. It is the highest PLQY reported for the nanocrystals to date. However, the $\text{Cs}_4\text{SnBr}_3\text{I}_3$ nanocrystals have emission at 601 nm and Cs_4SnI_6 at 578 nm. The possible reason for the unusual redshift of $\text{Cs}_4\text{SnBr}_3\text{I}_3$ is mixed halogen, which increases the lattice deformation energy [29]. Synthesized Cs_4SnI_6 nanocrystals have a PLQY of 27%. In this article, the thermodynamic stability of zero-dimensional and three-dimensional Sn-based materials are also studied comparatively. Density functional theory simulation is used to calculate enthalpies of formation ($\Delta_f H_m$). Zero-dimensional Cs_4SnBr_6 and Cs_4SnI_6 have negative values of -1721 , and -1496 kJ mol^{-1} , respectively, and three-dimensional CsSnBr_3 and CsSnI_3 have -642 and -522 kJ mol^{-1} , respectively. Therefore, zero-dimensional luminescent materials have more negative value than three-dimensional materials, making them more stable.

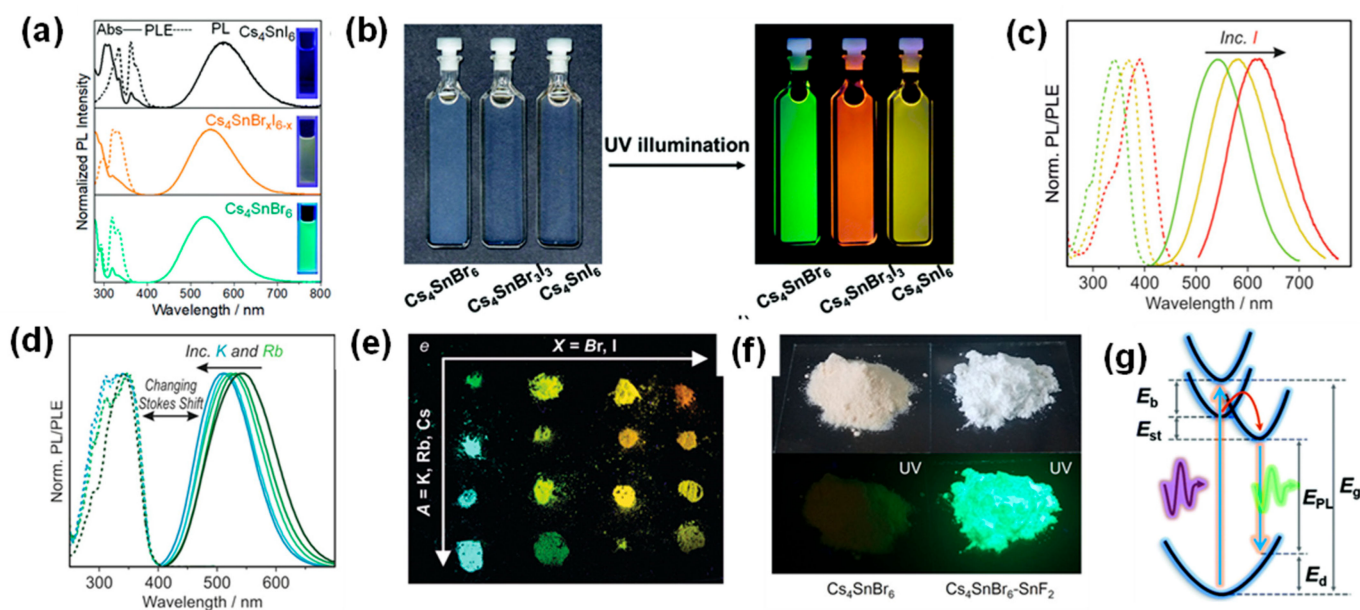


Figure 3. (a) Absorbance, photoluminescence excitation and emission spectra of Cs_4SnBr_6 , $\text{Cs}_4\text{SnBr}_6\text{I}_{6-x}$ and Cs_4SnI_6 . Reproduced with permission from [28], Copyright 2020, The Royal Society of Chemistry. (b) Normal and UV light images of Cs_4SnBr_6 , $\text{Cs}_4\text{SnBr}_3\text{I}_3$ and Cs_4SnI_6 . Reproduced with permission from [29], Copyright 2022, The Royal Society of Chemistry. (c) Photoluminescence excitation and emission spectra of $\text{Cs}_4\text{Sn}(\text{Br},\text{I})_6$. (d) Photoluminescence excitation and emission spectra of $\text{Cs}_{4-x}\text{A}_x\text{Sn}(\text{Br},\text{I})_6$, where $\text{A} = \text{K}^+, \text{Rb}^+$. (e) UV light image of $\text{Cs}_{4-x}\text{A}_x\text{Sn}(\text{Br},\text{I})_6$ powders. Reproduced with permission from [27], Copyright 2022, Wiley-VCH. (f) Normal and UV light image of Cs_4SnBr_6 and $\text{Cs}_4\text{SnBr}_6\text{-SnF}_2$. Reproduced with permission from [26], Copyright 2022, Wiley-VCH. (g) Schematic illustration of STE emission. Reproduced with permission from [29], Copyright 2022, The Royal Society of Chemistry.

Several studies have been carried out to understand the bulk of zero-dimensional Cs_4SnX_6 . The Kovalenko group used a solid-state synthesis method for Cs_4SnBr_6 and mixed it with cations (Rb^+ and K^+) and anions (I^-) [27]. In this method, CsBr and SnBr_2 were mixed in a stoichiometric ratio and heated in a vacuum at 360°C in the pellet. With tuning from the Br^- to I^- , the excitation and emission band redshift until the 50% substitution, as presented in Figure 3c. The emission band shifted from 540 to 620 nm for Cs_4SnBr_6 of $\text{Cs}_4\text{SnBr}_3\text{I}_3$, respectively, although no emission was observed at room temperature with more than 50% of substitutions. These results are similar to the reported results for nanocrystals in Figure 3b. The substitution of monovalent cations (Rb^+ and K^+) at the Cs^+ site blue shift the emission peak, as shown Figure 3d. Moreover, 25% substitution of Rb^+ and K^+ shift emission bands to 519 and 510 nm, respectively. They have studied the tunable emission in Cs_4SnBr_6 with different amounts of Rb^+ , K^+ , and I^- in UV light, as shown in Figure 3e. They obtained the highest quantum efficiency of 15% for Cs_4SnBr_6 . Recently Zhang et al. [26] synthesized Cs_4SnBr_6 powder by the ball mill method, and further oxidation was reduced by partial substitution by F^- , as shown in Figure 3f. The PLQY was enhanced from 2.8% to 62.8% after a partial substitution of F, which is the highest PLQY achieved for the bulk compound. F substitution at the Br site breaks the lattice symmetry by introducing lattice distortion in the octahedral, a possible reason for enhancing emission. Moreover, this research finds the reduction in charge transfer between oxygen and Sn^{2+} by calculating the Bader atomic charge [26]. The Bader charge gives information about the charge transfer between O_2 and Sn^{2+} [26]. Cs_4SnBr_6 has a Bader charge of 0.421e, and after F^- substitution, it changes to 0.299e, which accomplishes that charge transfer inhibition and resultantly suppresses oxidation.

Both nanocrystal and bulk crystals exhibit the possible emission mechanism of luminescence Cs_4SnBr_6 via STE in Figure 3g, and the emission energy can describe by the given equation for the mechanism.

$$E_{pl} = E_g - E_b - E_{STE} - E_d$$

E_{pl} is the photoluminescence energy, E_g is the bandgap, E_b binding energy, E_{STE} is self-trapping exciton energy, and E_d is lattice deformation energy.

All these studies regarding the Sn-based confirm that Cs_4SnBr_6 has green-emissive luminescent properties and can be a possible candidate for lighting applications.

2.2.2. Zn-Based

Zn-derived zero-dimensional luminescence materials are synthesized with different dopants. In Cs_2ZnCl_4 , $[\text{ZnCl}_4]^{2-}$ presents in the tetrahedral coordination with cation Cs^+ in the void. Although Cs_2ZnCl_4 does not emit light, doping induces the emission via self-trapped exciton emission. Wang et al. [30] used the acid precipitation method to synthesize Sn^{2+} -doped into Cs_2ZnCl_4 . Sn^{2+} has an outer cell electronic configuration of ns^2 , which resultantly have the possible transition from 1P_1 to 1S_0 and 3P_1 to 1S_0 . They observed the emission centered at 648 nm because of the transition from 3P_1 to 1S_0 . The theoretical calculation found isolated tetrahedral $[\text{ZnCl}_4]^{2-}$ possesses almost regular arrangement in Cs_2ZnCl_4 . Sn-doped Cs_2ZnCl_4 has disphenoidal $[\text{SnCl}_4]^{2-}$ units to capture the exciton for STE. Moreover, these systems have a binding energy of 15 meV, which is lower and insufficient for lighting applications. Although introducing organic cations increases the binding energy in a Zn-based system, we do not cover articles related to organic-inorganic hybrid materials in this review.

Zero-dimensional Cs_3ZnX_5 compounds are also developed in areas for lighting applications. Cs_3ZnX_5 ($x = \text{Cl}$ and Br) has a tetragonal crystal system with a space group of $I4/mcm$ where $[\text{ZnX}_4]^{2-}$ is in tetrahedral coordination [31]. The hot-injection method is used to synthesize the nanocrystals Cs_3ZnCl_5 and Cs_3ZnBr_5 . Cs_3ZnCl_5 emits 468 nm at the excitation wavelength of 275 nm, which shifts to 484 nm in Cs_3ZnBr_5 . Recently Liu et al. [32] used doping of Sb^{3+} in Cs_3ZnCl_5 , where Sb partially occupies the Zn positions. Doping of Sb^{3+} gives an emission from red to orange with increased dopant concentrations, as shown in Figure 4a. The compound has two excitation peaks because of the transition of $^1S_0 \rightarrow ^3P_1$ and $^1S_0 \rightarrow ^3P_1$ at 275 nm and 320 nm in Figure 4b. The emission after Sb^{3+} causes a broadband emission with large stock because of the STE at the emission center at 640 nm in Figure 4c. It is well-studied that the emission occurred via triplet self-trapped excitons in Sb^{3+} -doped systems. The PLQY of the Sb^{3+} -doped system achieved up to 34.18% at the excitation wavelength of 320 nm. However, this system can still be excitable by UV light and stability of this compound needs to be studied in detail. We have added comparative photo-physical properties of 0D metal halide with divalent units in Table 2.

2.2.3. Mn-Based

Manganese-derived luminescence material already attracts the researcher to green- and red-emissive materials Cs_3MnBr_5 and CsMnBr_3 . CsMnBr_3 are in one-dimensional electronic configuration with octahedral coordination and Cs_3MnBr_5 in zero-dimensional electronic configurations with tetrahedral coordination. Several groups used different types of nanocrystals, single crystals, and bulk crystals for Cs_3MnBr_5 and CsMnBr_3 . Nanocrystals are synthesized by hot injection, where cesium acetate and manganese acetate dissolve in a nonpolar solvent with organic ligands. Organic bromide ligand precursors were further added for complete reaction at a high temperature in the inert atmosphere to complete the reaction. It is noted that all nanocrystals are stored in a nonpolar solvent with additional organic ligands to stabilize them. Prof. Manna's group synthesized CsMnBr_3 , and Cs_3MnBr_5 nanocrystals doped with rare earth elements and found that CsMnBr_3 is the ideal compound to use as a sensitizer for energy transfer in rare earth elements [33].

They tuned the temperature and stoichiometric ratio of Cs_2CO_3 , manganese(II) acetate, and benzoyl bromide for the synthesizing of CsMnBr_3 and Cs_3MnBr_5 separately. The quantum efficiency for NIR-1 is very low, and it needs to be enhanced. Recently Almutlaq et al. synthesized CsMnBr_3 nanocrystals and achieved a PLQY of up to 56% [34]. Kong et al. used phase engineering to change the crystal structure with different emissions [35]. They used the hot-injection method with different ratios of precursors to synthesize Cs_3MnBr_5 and CsMnBr_3 emissions at 520 and 660 nm, respectively, as shown in Figure 5a. However, they found that the CsMnBr_3 can transform into Cs_3MnBr_5 after a reaction with isopropanol, and both the nanocrystals of CsMnBr_3 and Cs_3MnBr_5 can absorb water and transform into blue-emissive $\text{Cs}_2\text{MnBr}_4 \cdot 2\text{H}_2\text{O}$ at 440 nm. Although the PLQY of $\text{Cs}_2\text{MnBr}_4 \cdot 2\text{H}_2\text{O}$ is low, it can further transform into the mixture of Cs_3MnBr_5 and CsMnBr_3 after dehydration, as shown in Figure 5b,c. These recent studies found that the Mn-based material can be a possible candidate to replace lead halide perovskites for future optoelectronics applications. However, several studies needed to be carried out for industrial applications, such as the low PLQY of nanocrystals and the stability of these compounds.

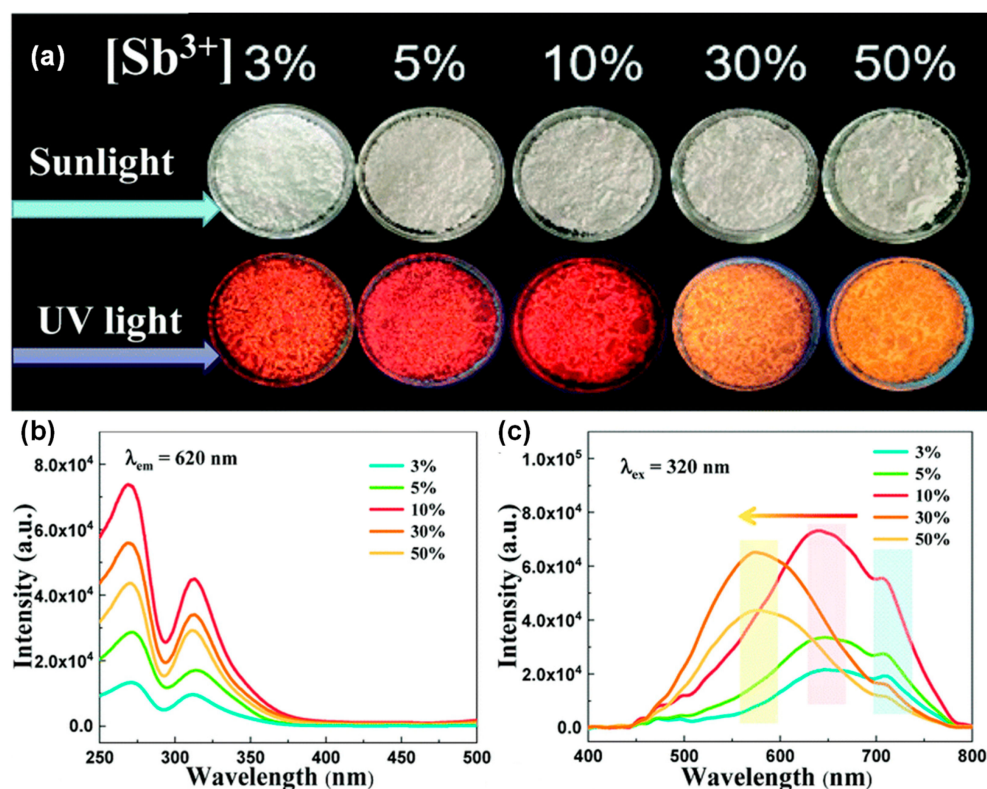


Figure 4. (a) Sunlight and UV light image of different amount of Sb^{3+} in Cs_3ZnCl_5 . (b) Photoluminescence excitation and (c) emission spectra for $\text{Cs}_3\text{ZnCl}_5:\text{Sb}^{3+}$ at 620 nm and 320 nm, respectively. Reproduced with permission from [32], Copyright 2022, The Royal Society of Chemistry.

Table 2. Properties of 0D metal halide with divalent units.

Formula	Method	Isolated Species	Em. Wave. (nm)	FWHM (nm)	PLQY (%)	Ref.
Cs_4SnBr_6 NC	Hot injection	$[\text{SnBr}_6]^{4-}$	537		52	[29]
Cs_4SnI_6 NC	Hot injection	$[\text{SnI}_6]^{4-}$	578		27	[29]
$\text{Cs}_4\text{SnBr}_6\text{-SnF}_2$	Ball Milling	$[\text{SnBr}_6]^{4-}$	540		62.8	[26]
Cs_3ZnCl_5	Hot injection	$[\text{ZnCl}_4]^{2-}$	484	79		[31]
Cs_3ZnBr_5	Hot injection	$[\text{ZnBr}_4]^{2-}$	468	76	7.98	[31]
Cs_3MnBr_5 NC	Hot injection	$[\text{MnBr}_4]^{2-}$	520	43	48	[35]
$\text{Cs}_2\text{MnBr}_4 \cdot 2\text{H}_2\text{O}$	injection/Humid environment	$[\text{MnBr}_4(\text{H}_2\text{O})_2]^{2-}$	440		1.29	[35]

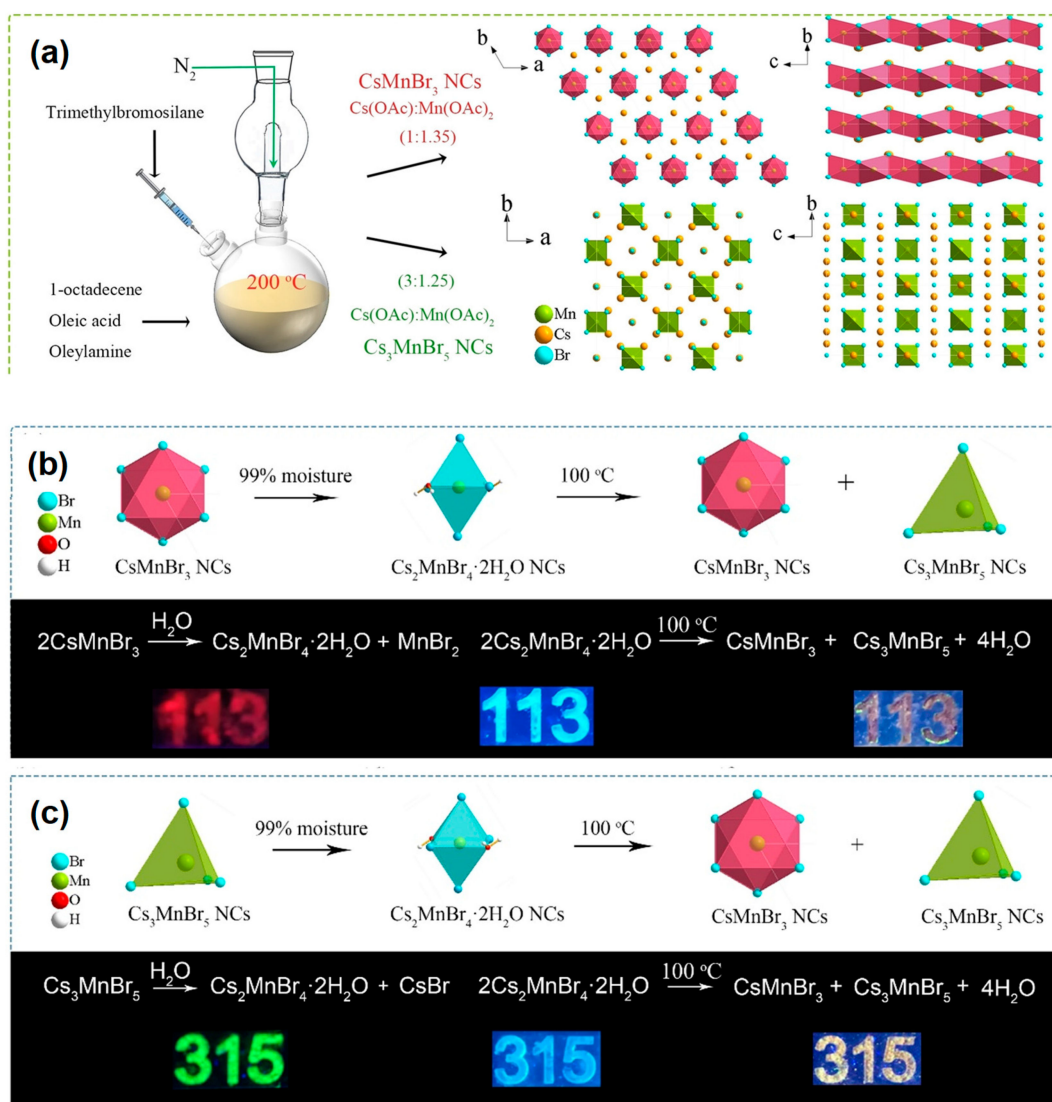


Figure 5. (a) Synthesis process for CsMnBr_3 and Cs_3MnBr_5 and their crystal structures, respectively. (b) Transformation of CsMnBr_3 to $\text{Cs}_2\text{MnBr}_4 \cdot 2\text{H}_2\text{O}$ in moisture (99%) and further transformation by dehydration to CsMnBr_3 and Cs_3MnBr_5 . (c) Transformation of Cs_3MnBr_5 to $\text{Cs}_2\text{MnBr}_4 \cdot 2\text{H}_2\text{O}$ in moisture (99%) and further transformation by dehydration to CsMnBr_3 and Cs_3MnBr_5 . Reproduced with permission from [35], Copyright 2021, Wiley-VCH.

2.3. Tri-Valent Coordinated Zero-Dimensional Materials

2.3.1. Bi-Based

Different kinds of Bi-derived inorganic luminescence materials are reported, such as zero-dimensional (Cs_3BiX_6) and two-dimensional ($\text{Cs}_3\text{Bi}_2\text{X}_9$) materials [36,37]. In Cs_3BiX_6 , $[\text{BiX}_6]^{3-}$ are in isolated octahedral coordination, and in $\text{Cs}_3\text{Bi}_2\text{X}_9$, the $[\text{BiX}_6]^{3-}$ octahedral coordination is attached to each other's to form layers. Cs_3BiCl_6 has a monoclinic phase with the $\text{C}2/c$ space group [38]. In this work, they also find the decomposition of Cs_3BiX_6 to $\text{Cs}_3\text{Bi}_2\text{X}_9$ at heating to 220°C . Cs_3BiCl_6 has broadband with emission centered at 391 nm. Cs_3BiCl_6 can further transform into an anion exchange reaction to Cs_3BiBr_6 ; by iodide exchange, it transforms into $\text{Cs}_3\text{Bi}_2\text{I}_9$. Along with it, zero-dimensional Cs_3BiX_6 can transform into $\text{Cs}_3\text{Bi}_2\text{X}_9$ after the insertion of BiX_3 . So far, Bi-based zero-dimensional material is not able to make tunable emissions. We have added comparative photo-physical properties of 0D metal halide with trivalent units in Table 3.

2.3.2. In-Based

Indium (In)-based zero-dimensional materials, such as Cs_3InBr_6 , $\text{Cs}_2\text{InCl}_5(\text{H}_2\text{O})$, $\text{Rb}_2\text{InCl}_5(\text{H}_2\text{O})$, and $\text{Cs}_2\text{InBr}_5(\text{H}_2\text{O})$, and doping with different dopants are reported in [39–43]. Cs_3InBr_6 nanocrystals were synthesized by the hot-injection method, and the material exhibits broadband luminescence at an emission of 450 nm in Figure 6a [42]. The emission was due to distortions in the $[\text{InBr}_6]^{3-}$ octahedral. Recently $\text{Cs}_2\text{InCl}_5(\text{H}_2\text{O})$, $\text{Rb}_2\text{InCl}_5(\text{H}_2\text{O})$, and $\text{Cs}_2\text{InBr}_5(\text{H}_2\text{O})$ compounds have also attracted interest, which makes them tunable emission with dopants. $\text{Rb}_2\text{InCl}_5(\text{H}_2\text{O})$ has $[\text{InCl}_5(\text{H}_2\text{O})]^{2-}$ an isolated octahedral coordinate (In) with the orthorhombic crystal system of the Pnma space group [39]. The material has low photoluminescence quantum yield due to parity forbidden transition and parity broken after substitution of Sb^{3+} at the In^{3+} site. Resultantly, the PLQY of $\text{Rb}_2\text{InCl}_5(\text{H}_2\text{O})$ enhances from 1 to 90% after Sb^{3+} doping at the emission center at 600 nm, which makes a yellow emission. Furthermore, $\text{Rb}_3\text{InCl}_6:\text{Sb}$ shows a green emission at 497 nm with a PLQY of 95%, as shown in Figure 6b. These results attribute the blue shift in the STE state of $\text{Rb}_3\text{InCl}_6:\text{Sb}$ compared to $\text{Rb}_2\text{InCl}_5\cdot\text{H}_2\text{O}:\text{Sb}$. The luminescence shifts with the change in STE states. Zhou et al. [40] synthesized a $\text{Cs}_3\text{InBr}_5(\text{H}_2\text{O})$ single crystal with a quantum yield of 33%, as shown in Figure 6c. Figure 6d shows red light emission centered at 695 nm with UV excitation.

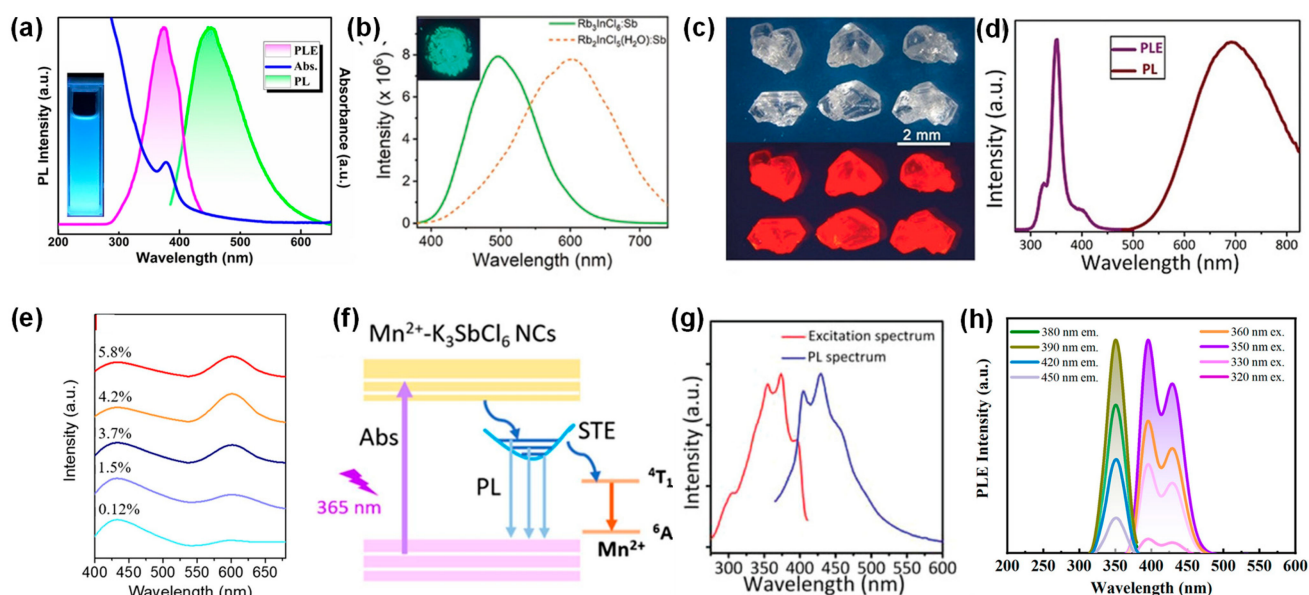


Figure 6. (a) UV–vis, photoluminescence excitation, and emission spectra of Cs_3InBr_6 nanocrystals in solution. Reproduced with permission from [42], Copyright 2021, Elsevier. (b) Photoluminescence emission spectra of $\text{Rb}_3\text{InCl}_6:\text{Sb}$ and $\text{Rb}_2\text{InCl}_5(\text{H}_2\text{O}):\text{Sb}$. Reproduced with permission from [39], Copyright 2020, Wiley–VCH (c) Ambient and UV light image of $\text{Cs}_2\text{InBr}_5\cdot\text{H}_2\text{O}$ (d) Photoluminescence excitation ($\lambda_{\text{em}} = 695 \text{ nm}$) and emission ($\lambda_{\text{ex}} = 355 \text{ nm}$) spectra of $\text{Cs}_2\text{InBr}_5\cdot\text{H}_2\text{O}$. Reproduced with permission from [40], Copyright 2019, Wiley–VCH. (e) Photoluminescence emission spectra of K_3SbCl_6 with Mn^{2+} doping (0.12%, 1.5%, 3.7%, 4.2%, and 5.8%). (f) Mechanism of energy transfer of self-trapped exciton emission to Mn^{2+} . Reproduced with permission from [44], Copyright 2021, Elsevier. (g) Photoluminescence excitation ($\lambda_{\text{em}} = 429 \text{ nm}$) and emission ($\lambda_{\text{ex}} = 355 \text{ nm}$) spectra of Cs_3YbBr_6 nanocrystal. Reproduced with permission from [45], Copyright 2022, Wiley–VCH. (h) Photoluminescence excitation and emission spectra of Cs_3CeBr_6 nanocrystals at different excitation and emission wavelength. Reproduced with permission from [16], Copyright 2021, the American Chemical Society.

Table 3. Properties of 0D metal halide with trivalent units.

Formula	Method	Isolated Species	Em. Wave. (nm)	FWHM (nm)	PLOY (%)	Ref.
Cs ₃ BiCl ₆ NC	Hot injection	[BiCl ₆] ^{3−}	391	60		[38]
Cs ₃ Bi ₂ Br ₉	Hot injection	[BiBr ₆] ^{3−}	468	40	4.5%	[37]
Cs ₃ InBr ₆ NC	Hot injection	[InBr ₆] ^{3−}	450	~100	22.3%	[42]
Cs ₂ InBr ₅ (H ₂ O)	Temperature-lowering crystallization	[InBr ₅ (H ₂ O)] ^{2−}	695		33%	[40]
K ₃ SbCl ₆ NC	Hot injection	[SbCl ₆] ^{3−}	440	102	22.3%	[44]
Cs ₃ YbCl ₆	Heating-up	[YbCl ₆] ^{3−}	429	76	59.8%	[45]
Cs ₃ CeBr ₆ SC	Solid state	[CeBr ₆] ^{3−}	391, 421		92.5%	[16]

2.3.3. Sb-Based

Antimony (Sb)-based zero-dimensional materials such as K₃SbCl₆ and Rb₇Sb₃Cl₁₆ doping with different dopants are reported [44,46,47]. K₃SbCl₆ nanocrystals were synthesized by hot-injection method with Mn²⁺ dopant [44]. Pristine K₃SbCl₆ nanocrystal has a monoclinic crystal system where isolated [SbCl₆]^{3−} octahedral are surrounded by K⁺ ions. Pristine K₃SbCl₆ has blue emission centered at 440 nm with a quantum yield of 22.3%. Mn²⁺ substitute Sb³⁺ in octahedral coordination gives emission at 600 nm by ⁴T₁ – ⁶A₁ transition by energy transfer (Figure 6e). Figure 6f represents the possible energy transfer from STE to Mn²⁺. The white LED was fabricated further on a UV chip with K₃SbCl₆:Mn²⁺ nanocrystals with single materials. Also, zero-dimensional Rb₇Sb₃Cl₁₆ nanocrystals are synthesized, exhibiting yellow broadband emission at 567 nm [46]. Pinchetti et al. used Rb₇Sb₃Cl₁₆ nanocrystals doped with Mn²⁺ showing energy transfer and magnetic properties [47]. These results are attributed to the STE-derived energy transfer to Mn²⁺. The material with low doping shows paramagnetic nature, and an increased amount of dopant changes it to antiferromagnetic nature.

2.3.4. Rare-Earth-Based

Rare earth trivalent cations can occupy the B site with the octahedral units. So far, only articles report the synthesis of Cs₃LnCl₆ (Ln = Y, Ce, Gd, Er, Tm, and Yb) nanocrystals by the heating-up method [45]. In this method, both precursors are mixed with oleic acid and oleylamine ligand with the nonpolar solvent. The reaction was first heated at 130 °C to remove water content from nonpolar solvent and then heated at 270 °C to complete the formation of nanocrystals. All compound shows the highest quantum efficiency for blue light. Figure 6g shows the emission of Cs₃YbCl₆ centered at 429 nm at the excitation of 355 nm with the quantum efficiency of 59.8%. These results suggest zero-dimensional compounds are materials that can be made with rare earth elements. However, further study is needed on their characteristic emissions in the infrared region. So far, only CsMnBr₃ is the ideal sensitizer material to transfer energy to rare-earth elements [33].

Wang et al. also report the synthesis of Cs₃CeBr₆ with a quantum efficiency of up to 90% for powder and thin film [16]. Cs₃CeBr₆ has orthorhombic crystal systems with the Pbcm space group. The solid-state method is used to synthesize powder of Cs₃CeBr₆ with isolated [CeBr₆]^{3−} in octahedral coordination. Thin films of Cs₃CeBr₆ were fabricated by thermal evaporation of CsBr and CeBr₃. The Cs₃CeBr₆ system has dual emissions at 391 and 421 nm due to the transition between Ce 5d Figure 6h, and the external quantum efficiency of Cs₃CeBr₆ was recorded at a maximum of up to 0.46%.

3. Application of Zero-Dimensional Materials

The zero-dimensional materials are used for several optoelectronics applications, such as a light-emitting diode, ultrafast switching memory, photodetector, and scintillators.

3.1. Light-Emitting Diode

The white light-emitting diode is fabricated on a UV chip using zero-dimensional materials, as shown in Figure 7a,b. High luminescence green-emissive Cs_4SnBr_6 are mixed with blue- and red-emissive phosphors $\text{BaMgAl}_{10}\text{O}_{17}:\text{Eu}^{2+}$ and $\text{CaAlSiN}_3:\text{Eu}^{2+}$ to generate white light, as shown in Figure 7b, respectively. The fabricated devices have a color-rendering index of 96% with CIE coordinates of (0.34, 0.33) at 20 mA. The driving current increased to 200 mA, and only the color rendering index was reduced to 86%, making the device stable. The device was continuously operated at 1000 h, the color rendering index remained unchanged, and the relative luminous efficiency was reduced by up to 79%. Along with it, the CIE coordinate only shift from (0.34, 0.33) to (0.33, 0.32) after 1000 h. These results show that the Cs_4SnBr_6 -prepared device has excellent operation stability. Xu et al. [29] also reported a device using Cs_4SnBr_6 nanocrystals with red- and green-emissive phosphors and achieved a color rendering index of 92%.

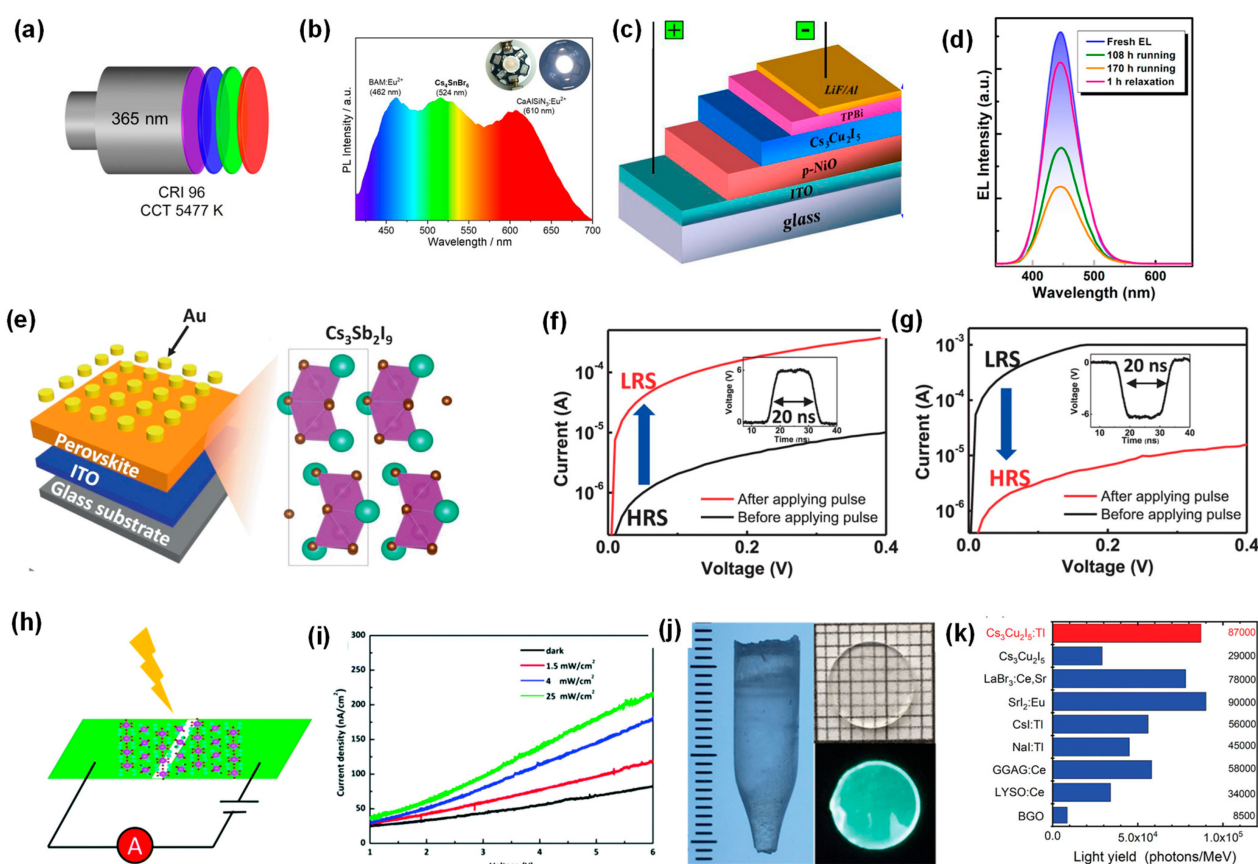


Figure 7. (a) Schematic diagram of LED devices based on Cs_4SnBr_6 - SnF_2 . (b) Emission spectra of the fabricated white light diode (WLED) by blue-emissive $\text{BaMgAl}_{10}\text{O}_{17}:\text{Eu}^{2+}$, green-emissive Cs_4SnBr_6 - SnF_2 and red-emissive $\text{CaAlSiN}_3:\text{Eu}^{2+}$ phosphors. Reproduced with permission from [26], Copyright 2022, Wiley-VCH. (c) Schematic diagram of blue light-emitting diode (LED) made by $\text{Cs}_3\text{Cu}_2\text{I}_5$ nanocrystals. (d) Electroluminescence spectra of $\text{Cs}_3\text{Cu}_2\text{I}_5$ nanocrystals made blue LED device for fresh and at different time intervals. Reproduced with permission from [20], Copyright 2020, the American Chemical Society. (e) Schematic diagram of resistive switching memory made by $\text{Cs}_3\text{Sb}_2\text{I}_9$. I-V curve of resistive switching memory made (f) set pulse (g) reset pulse. Reproduced with permission from [48], Copyright 2021, the Nature Publishing Group. (h) Schematic diagram of Photodetector device made by Cs_3BiBr_6 . (i) I-V characteristic of photodetector device at different power densities. Reproduced with permission from [49], Copyright 2019, Royal Society of Chemistry) (j) TI-doped $\text{Cs}_3\text{Cu}_2\text{I}_5$ crystal grown by Bridgman method. (k) Comparison with different scintillators. Reproduced with permission from [50], Copyright 2021, Wiley-VCH.

Lead-free copper-based zero-dimensional material is a possible candidate for blue light-emitting diode application because of the high quantum yield at the emission center at ~ 450 nm [20]. $\text{Cs}_3\text{Cu}_2\text{I}_5$ nanocrystals are used for deep blue LED and have achieved external quantum efficiency of up to 1.12%. As shown in Figure 7c,d, the device was fabricated with an active layer of $\text{Cs}_3\text{Cu}_2\text{I}_5$ nanocrystal with 1,3,5-tri(phenyl-2-benzimidazolyl)-benzene (TP) as the electron injecting layer and NiO as the hole injecting layer for the device. The fabricated device has a coordinate of (0.16, 0.07) for blue LED with NTSC standards. The device was operated for 170 h, and after 1 h of relaxation, electroluminescence almost recovered to the initial level, which indicates the stability of the devices. These recent studies suggest the use of zero-dimensional material for WLED and blue LED.

3.2. Ultrafast Switching Memory

Lead halide perovskite is developed as the ideal candidate for resistive switching memory because of multilevel data storage and low operational voltage [51,52]. Halide perovskites have applied resistive switching because of the presence of halide defects or migration of ions [48]. Toxicity and stability issues mean that lead is not environment friendly for further application. $\text{Cs}_3\text{Sb}_2\text{I}_5$ -based resistive switching memory was fabricated, as shown in Figure 7e [48]. The electrical signals are recorded by applying a voltage at Au when ITO is grounded. Figure 7f,g showed the I-V characteristics of the device when the applied voltage was set at 6 V with a width of 20 ns and a reset voltage of -6 V with a width of 20 ns. To find the fast switching, bias voltage was used from 0 to 0.4 V to find the resistance state before and after the pulse. With the applied positive voltage pulse, the state changes from a high-resistance state to a low-resistance state, and further negative voltage pulse shifts the state and vice versa. All these results confirm that the $\text{Cs}_3\text{Sb}_2\text{I}_5$ -based device can be operated with a fast switching speed of 20 ns. So far, only $\text{Cs}_3\text{Sb}_2\text{I}_5$ has been applied for fast-switching memory applications.

3.3. Photodetectors and Scintillators

After using CsPbX_3 and lead-free double perovskite for photodetector applications, zero-dimensional Cs_3BiBr_6 lead-free luminescent materials were used to detect UV-Vis light [49]. Cs_3BiBr_6 was deposited on the ITO substrate, and the photocurrent was measured at the bias voltage of 6V by 400 nm monochromatic illumination, as shown in Figure 7h. The fabricated device has 0.3 nA dark current and increases with an increasing power density, as shown in Figure 7i. The fabricated device has responsivity and detectivity of ~ 25 mA W^{-1} and $\sim 0.8 \times 10^9$ Jones, respectively. Highly crystalline zero-dimensional materials could be ideal for detection application in UV light with a high PLQY.

Scintillators convert high energy χ -ray, γ -ray, and α particles into low energy UV- visible light. Recently doped and un-doped $\text{Cs}_3\text{Cu}_2\text{I}_5$ were used for χ -ray and γ -ray detections [22,50,53]. Perovskite has high photoluminescence quantum yield and high effective atomic number, making it a more suitable candidate for scintillator application. The Bridgman method is used to synthesize the single crystal, as shown in Figure 7j [50]. $\text{Cs}_3\text{Cu}_2\text{I}_5$ has a high quantum yield of 68% at an emission center of ~ 450 nm, and further doping with Tl and In-enhanced it to 79.2% and 88.4%, respectively. Single crystal of $\text{Cs}_3\text{Cu}_2\text{I}_5:\text{Tl}$ has a scintillation yield of 1,50,000 photons/MeV with a detection limit of 66.3 nGy_{air}s⁻¹. Additionally, $\text{Cs}_3\text{Cu}_2\text{I}_5:\text{Tl}$ single crystal has a scintillation yield of 87,000 photons/MeV under ¹³⁷Cs γ -ray detection, as shown in Figure 7k [50]. The In-doped $\text{Cs}_3\text{Cu}_2\text{I}_5$ obtained a scintillation yield of 53,000 photons/MeV for χ -ray [22]. These results show that $\text{Cs}_3\text{Cu}_2\text{I}_5$ highly crystalline materials can be used for high-energy photon detections.

4. Conclusions and Outlook

Lead halide perovskite's toxicity and stability issues concern finding an alternative with similar properties. Tin could be alternative to replace Pb, although it is not stable and oxidizes in contact with the environment. Several research groups worked on Lead-

free double perovskite, which has broadband emission and is excitable by UV light. So far, octahedral and tetrahedral coordinated luminescence materials have been reported with different applications. The challenges and perspectives regarding zero-dimensional discussed as follows:

1. Copper-derived $\text{Cs}_3\text{Cu}_2\text{I}_5$ has emission at ~ 445 nm, and the quantum yield increased to $\sim 88\%$. This system also exhibits external quantum efficiency of $\sim 1.12\%$ and further improvement will make it a promising candidate for deep blue LEDs. However, further improvement in the future is needed to improve the quantum efficiency. Along with LED, these compounds are widely applied for χ -ray scintillation, where $\text{Cs}_3\text{Cu}_2\text{I}_5$: Tl has a higher scintillation yield than CsI: Tl.
2. Bimetallic Cs-Ag-X systems emission can be tuned with the change in the crystallographic dimensions and halides. However, these systems achieved high quantum yields between 17 and 68% but need to be excited by the UV light. This concern restricts the use of the material for LED. Along with these bi-metallic systems, Bi-based $\text{Cs}_3\text{Bi}_2\text{X}_9$ nanocrystals are reported but suffer from a very low quantum yield of up to 4.5% only.
3. The Quantum efficiency of Cs_4SnBr_6 enhanced achieved up to $\sim 62\%$, making it the ideal material for LED applications with high stability. However, the material can only be excitable by UV chip for WLED, so the stability of the Cs_4SnX_6 needed to be detail study.
4. Cs_3MnBr_5 and CsMnBr_3 have green and red light emissions with tetrahedral and octahedral coordination, respectively. These materials have emissions around ~ 520 nm and ~ 620 nm, which are ideal for lighting applications. However, further research is needed to enhance quantum efficiency and stability for industrial applications. The hot-injection method is complicated for the nanocrystal, and further research is needed to improve the process.
5. So far, these zero-dimensional materials are applied for several applications discussed in the application sections. However, these materials could be applied for solar cells, photo-catalysis, and sensing applications.

Finally, several zero-dimensional materials are studied but still need deep fundamental research to develop materials for optoelectronics industries in the future. Ag, Bi, and Mn-based compounds have tunable emissions but must improve the emission properties for real applications.

Author Contributions: Conceptualization, K.D., W.-T.H. and R.-S.L.; writing—review and editing, K.D., W.-T.H. and R.-S.L.; visualization, K.D. and W.-T.H.; supervision, R.-S.L.; project administration, R.-S.L.; funding acquisition, R.-S.L. All authors have read and agreed to the published version of the manuscript.

Funding: This work was financially supported by the National Science and Technology Council in Taiwan (contract NSTC 109-2113-M-002-020-MY3).

Data Availability Statement: Not applicable.

Conflicts of Interest: The authors declare no conflict of interest.

References

1. Protesescu, L.; Yakunin, S.; Bodnarchuk, M.I.; Krieg, F.; Caputo, R.; Hendon, C.H.; Yang, R.X.; Walsh, A.; Kovalenko, M.V. Nanocrystals of Cesium Lead Halide Perovskites (CsPbX_3 , X = Cl, Br, and I): Novel Optoelectronic Materials Showing Bright Emission with Wide Color Gamut. *Nano Lett.* **2015**, *15*, 3692–3696. [[CrossRef](#)] [[PubMed](#)]
2. Swarnkar, A.; Marshall, A.R.; Sanehira, E.M.; Chernomordik, B.D.; Moore, D.T.; Christians, J.A.; Chakrabarti, T.; Luther, J.M. Quantum Dot-Induced Phase Stabilization of α - CsPbI_3 Perovskite for High-Efficiency Photovoltaics. *Science* **2016**, *354*, 92–95. [[CrossRef](#)] [[PubMed](#)]
3. Dave, K.; Bao, Z.; Nakahara, S.; Ohara, K.; Masada, S.; Tahara, H.; Kanemitsu, Y.; Liu, R.S. Improvement in Quantum Yield by Suppression of Trions in Room Temperature Synthesized CsPbBr_3 Perovskite Quantum Dots for Backlight Displays. *Nanoscale* **2020**, *12*, 3820–3826. [[CrossRef](#)] [[PubMed](#)]

4. Dou, L.; Yang, Y.; You, J.; Hong, Z.; Chang, W.H.; Li, G.; Yang, Y. Solution-processed Hybrid Perovskite Photodetectors with High detectivity. *Nat. Commun.* **2014**, *5*, 5404. [[CrossRef](#)] [[PubMed](#)]
5. Dave, K.; Fang, M.H.; Bao, Z.; Fu, H.T.; Liu, R.S. Recent Developments in Lead-Free Double Perovskites: Structure, Doping, and Applications. *Chem. Asian J.* **2020**, *15*, 242–252. [[CrossRef](#)]
6. Gupta, S.; Bendikov, T.; Hodes, G.; Cahen, D. CsSnBr₃, A Lead-Free Halide Perovskite for Long Term Solar Cell Application: Insights on SnF₂ Addition. *ACS Energy Lett.* **2016**, *1*, 1028–1033. [[CrossRef](#)]
7. Luo, J.; Wang, X.; Li, S.; Liu, J.; Guo, Y.; Niu, G.; Yao, L.; Fu, Y.; Gao, L.; Dong, Q.; et al. Efficient and Stable Emission of Warm–White Light from Lead–Free Halide Double Perovskites. *Nature* **2018**, *563*, 541–545. [[CrossRef](#)]
8. Dave, K.; Huang, W.T.; Leśniewski, T.; Lazarowska, A.; Jankowski, D.; Mahlik, S.; Liu, R.S. Photoluminescence Enhancement Study in a Bi-doped Cs₂AgInCl₆ Double Perovskite by Pressure and Temperature-dependent Self-Trapped Exciton Emission. *Dalton Trans.* **2022**, *51*, 2026–2032. [[CrossRef](#)]
9. Li, M.; Xia, Z. Recent Progress of Zero-Dimensional Luminescent Metal Halides. *Chem. Soc. Rev.* **2021**, *50*, 2626–2662. [[CrossRef](#)]
10. Wang, L.; Liu, H.; Zhang, Y.; Mohammed, O.F. Photoluminescence Origin of Zero-Dimensional Cs₄PbBr₆ Perovskite. *ACS Energy Lett.* **2020**, *5*, 87–99. [[CrossRef](#)]
11. Zhou, C.; Lin, H.; He, Q.; Xu, L.; Worku, M.; Chaaban, M.; Lee, S.; Shi, X.; Du, M.H.; Ma, B. Low dimensional metal halide perovskites and hybrids. *Mater. Sci. Eng. R Rep.* **2019**, *137*, 38–65. [[CrossRef](#)]
12. Zhou, C.; Xu, L.J.; Lee, S.; Lin, H.; Ma, B. Recent Advances in Luminescent Zero-Dimensional Organic Metal Halide Hybrids. *Adv. Optical Mater.* **2021**, *9*, 2001766. [[CrossRef](#)]
13. Schubert, E.F. *Light-Emitting Diodes*; Schubert, E.F., Ed.; Rensselaer Polytechnic Institute: New York, NY, USA, 2018.
14. Zhou, L.; Liao, J.F.; Kuang, D.B. An Overview for Zero-Dimensional Broadband Emissive Metal-Halide Single Crystals. *Adv. Optical Mater.* **2021**, *9*, 2100544. [[CrossRef](#)]
15. Song, K.W.; Williams, R.T. *Self-Trapped Excitons*; Springer Science & Business Media: Berlin, Germany, 2013; Volume 105.
16. Wang, L.; Guo, Q.; Duan, J.; Xie, W.; Ji, G.; Li, S.; Chen, C.; Li, J.; Yang, L.; Tan, Z.; et al. Exploration of Nontoxic Cs₃CeBr₆ for Violet Light-Emitting Diodes. *ACS Energy Lett.* **2021**, *6*, 4245–4254. [[CrossRef](#)]
17. Li, S.; Luo, J.; Liu, J.; Tang, J. Self-Trapped Excitons in All-Inorganic Halide Perovskites: Fundamentals, Status, and Potential Applications. *J. Phys. Chem. Lett.* **2019**, *10*, 1999–2007. [[CrossRef](#)]
18. Fowler, W.B.; Marrone, M.J.; Kabler, M.N. Theory of Self-Trapped Exciton Luminescence in Halide Crystals. *Phys. Rev. B* **1973**, *8*, 5909–5919. [[CrossRef](#)]
19. Liu, X.; Yu, Y.; Yuan, F.; Zhao, C.; Dong, H.; Jiao, B.; Wu, Z. Vacuum Dual-Source Thermal-Deposited Lead-Free Cs₃Cu₂I₅ Films with High Photoluminescence Quantum Yield for Deep-Blue Light-Emitting Diodes. *ACS Appl. Mater. Interfaces* **2020**, *12*, 52967–52975. [[CrossRef](#)]
20. Wang, L.; Shi, Z.; Ma, Z.; Yang, D.; Zhang, F.; Ji, X.; Wang, M.; Chen, X.; Na, G.; Chen, S.; et al. Colloidal Synthesis of Ternary Copper Halide Nanocrystals for High-Efficiency Deep-Blue Light-Emitting Diodes with a Half-Lifetime above 100 h. *Nano Lett.* **2020**, *20*, 3568–3576. [[CrossRef](#)]
21. Rocanova, R.; Yangui, A.; Nhalil, H.; Shi, H.; Du, M.H.; Saporov, B. Near-Unity Photoluminescence Quantum Yield in Blue-Emitting Cs₃Cu₂Br_{5-x}I_x (0 ≤ x ≤ 5). *ACS Appl. Electron. Mater.* **2019**, *1*, 269–274. [[CrossRef](#)]
22. Wang, Q.; Zhou, Q.; Nikl, M.; Xiao, J.; Kucerkova, R.; Beitlerova, A.; Babin, V.; Prusa, P.; Linhart, V.; Wang, J.; et al. Highly Resolved X-Ray Imaging Enabled by In(I) Doped Perovskite-Like Cs₃Cu₂I₅ Single Crystal Scintillator. *Adv. Opt. Mater.* **2022**, *10*, 2200304. [[CrossRef](#)]
23. Huang, X.; Sun, Q.; Devakumar, B. Facile Low-temperature Solid-state Synthesis of Efficient Blue-emitting Cs₃Cu₂I₅ Powder Phosphors for Solid-state Lighting. *Mater. Today Chem.* **2020**, *17*, 100288. [[CrossRef](#)]
24. Zhang, Z.; Zhao, R.; Teng, S.; Huang, K.; Zhang, L.; Wang, D.; Yang, W.; Xie, R.; Pradhan, N. Color Tunable Self-Trapped Emissions from Lead-Free All Inorganic IA-IB Bimetallic Halides Cs-Ag-X (X = Cl, Br, I). *Small* **2020**, *16*, 2004272. [[CrossRef](#)] [[PubMed](#)]
25. Zhang, M.; Wang, X.; Yang, B.; Zhu, J.; Niu, G.; Wu, H.; Yin, L.; Du, X.; Niu, M.; Ge, Y.; et al. Metal Halide Scintillators with Fast and Self-Absorption-Free Defect-Bound Excitonic Radioluminescence for Dynamic X-Ray Imaging. *Adv. Funct. Mater.* **2021**, *31*, 2007921. [[CrossRef](#)]
26. Zhang, Q.; Liu, S.; He, M.; Zheng, W.; Wan, Q.; Liu, M.; Liao, X.; Zhan, W.; Yuan, C.; Liu, J.; et al. Stable Lead-Free Tin Halide Perovskite with Operational Stability >1200 h by Suppressing Tin(II) Oxidation. *Angew. Chem.* **2022**, *61*, e202205463.
27. Benin, B.M.; Dirin, D.N.; Morad, V.; Wörle, M.; Yakunin, S.; Rainò, G.; Nazarenko, O.; Fischer, M.; Infante, I.; Kovalenko, M.V. Highly Emissive Self-Trapped Excitons in Fully Inorganic Zero-Dimensional Tin Halides. *Angew. Chem. Int. Ed.* **2018**, *57*, 11329–11333. [[CrossRef](#)]
28. Tan, L.; Wang, W.; Li, Q.; Luo, Z.; Zou, C.; Tang, M.; Zhang, L.; He, J.; Quan, Z. Colloidal Syntheses of Zero-Dimensional Cs₄SnX₆ (X = Br, I) Nanocrystals with High Emission Efficiencies. *Chem. Commun.* **2020**, *56*, 387–390. [[CrossRef](#)]
29. Xu, K.; Wei, Q.; Wang, H.; Yao, B.; Zhou, W.; Gao, R.; Chen, H.; Li, H.; Wang, J.; Ning, Z. The 3D-Structure-Mediated Growth of Zero-Dimensional Cs₄SnX₆ Nanocrystals. *Nanoscale* **2022**, *14*, 2248–2255. [[CrossRef](#)]
30. Wang, X.; Shen, Q.; Chen, Y.; Ali, N.; Ren, Z.; Bi, G.; Wu, H. Self-Trapped Exciton Emission in an Sn(ii)-Doped all-Inorganic Zero-Dimensional Zinc Halide Perovskite Variant. *Nanoscale* **2021**, *13*, 15285–15291. [[CrossRef](#)]
31. Zhao, H.; Wei, Y.; Chen, Y.; Liu, C.; Jiang, F.; Liu, Y.; Hong, M. Blue-Emitting 0D Cs₃ZnX₅ (X = Cl, Br) Perovskite Nanocrystals Based on Self-Trapped Excitons. *J. Lumin.* **2022**, *249*, 119048. [[CrossRef](#)]

32. Liu, X.; Zhang, W.; Xu, R.; Tu, J.; Fang, G.; Pan, Y. Bright Tunable Luminescence of Sb³⁺ Doping in Zero-Dimensional Lead-Free Halide Cs₃ZnCl₅ Perovskite Crystals. *Dalton Trans.* **2022**, *51*, 10029–10035. [[CrossRef](#)]
33. Bahmani Jalali, H.; Pianetti, A.; Zito, J.; Imran, M.; Campolucci, M.; Ivanov, Y.P.; Locardi, F.; Infante, I.; Divitini, G.; Brovelli, S.; et al. Cesium Manganese Bromide Nanocrystal Sensitizers for Broadband Vis-to-NIR Downshifting. *ACS Energy Lett.* **2022**, *7*, 1850–1858. [[CrossRef](#)]
34. Almutlaq, J.; Mir, W.J.; Gutiérrez Arzaluz, L.; Yin, J.; Vasylevskiy, S.; Maity, P.; Liu, J.; Naphade, R.; Mohammed, O.F.; Bakr, O.M. CsMnBr₃: Lead-Free Nanocrystals with High Photoluminescence Quantum Yield and Picosecond Radiative Lifetime. *ACS Mater. Lett.* **2021**, *3*, 290–297. [[CrossRef](#)]
35. Kong, Q.; Yang, B.; Chen, J.; Zhang, R.; Liu, S.; Zheng, D.; Zhang, H.; Liu, Q.; Wang, Y.; Han, K. Phase Engineering of Cesium Manganese Bromides Nanocrystals with Color-Tunable Emission. *Angew. Chem.* **2021**, *60*, 19653–19659. [[CrossRef](#)]
36. Yang, H.; Cai, T.; Dube, L.; Chen, O. Synthesis of Double Perovskite and Quadruple Perovskite Nanocrystals Through Post-Synthetic Transformation Reactions. *Chem. Sci.* **2022**, *13*, 4874–4883. [[CrossRef](#)]
37. Yang, B.; Chen, J.; Hong, F.; Mao, X.; Zheng, K.; Yang, S.; Li, Y.; Pullerits, T.; Deng, W.; Han, K. Lead-Free, Air-Stable All-Inorganic Cesium Bismuth Halide Perovskite Nanocrystals. *Angew. Chem. Int. Ed.* **2017**, *56*, 12471–12475. [[CrossRef](#)]
38. Yang, H.; Cai, T.; Liu, E.; Hills-Kimball, K.; Gao, J.; Chen, O. Synthesis and Transformation of Zero-Dimensional Cs₃BiX₆ (X = Cl, Br) Perovskite-Analogue Nanocrystals. *Nano Res.* **2020**, *13*, 282291. [[CrossRef](#)]
39. Han, P.; Luo, C.; Yang, S.; Yang, Y.; Deng, W.; Han, K. All-Inorganic Lead-Free 0D Perovskites by a Doping Strategy to Achieve a PLQY Boost from <2% to 90%. *Angew. Chem. Int. Ed.* **2020**, *59*, 12709–12713.
40. Zhou, L.; Liao, J.F.; Huang, Z.G.; Wei, J.H.; Wang, X.D.; Li, W.G.; Chen, H.Y.; Kuang, D.B.; Su, C.Y. A Highly Red-Emissive Lead-Free Indium-Based Perovskite Single Crystal for Sensitive Water Detection. *Angew. Chem. Int. Ed.* **2019**, *58*, 5277–5281. [[CrossRef](#)]
41. Chang, T.; Wang, H.; Gao, Y.; Cao, S.; Zhao, J.; Zou, B.; Zeng, R. Component Engineering to Tailor the Structure and Optical Properties of Sb-Doped Indium-Based Halides. *Inorg. Chem.* **2022**, *61*, 1486–1494. [[CrossRef](#)]
42. Zhang, F.; Yang, D.; Shi, Z.; Qin, C.; Cui, M.; Ma, Z.; Wang, L.; Wang, M.; Ji, X.; Chen, X.; et al. Stable Zero-Dimensional Cesium Indium Bromide Hollow Nanocrystals Emitting Blue Light from Self-Trapped Excitons. *Nano Today* **2021**, *38*, 101153. [[CrossRef](#)]
43. Wei, J.H.; Luo, J.B.; Liao, J.F.; Ou, W.T.; Kuang, D.B. Te⁴⁺-Doped Cs₂InCl₅·H₂O Single Crystals for Remote Optical Thermometry. *Sci. China Mater.* **2022**, *65*, 764–772. [[CrossRef](#)]
44. Shao, H.; Wu, X.; Zhu, J.; Xu, W.; Xu, L.; Dong, B.; Hu, J.; Dong, B.; Bai, X.; Cui, H.; et al. Mn²⁺ Ions Doped Lead-Free Zero-Dimensional K₃SbCl₆ Perovskite Nanocrystals Towards White Light Emitting Diodes. *Chem. Eng. J.* **2021**, *413*, 127415. [[CrossRef](#)]
45. Pinchetti, V.; Moro, F.; Zhang, B.; Fanciulli, M.; De Trizio, L.; Meinardi, F.; Manna, L.; Brovelli, S. Magnetic Transitions and Energy Transfer Processes in Sb-Based Zero-Dimensional Metal Halide Nanocrystals Doped with Manganese. *ACS Energy Lett.* **2022**, *7*, 1566–1573. [[CrossRef](#)]
46. Shao, T.; Fang, Y.; He, C.; Zhang, L.; Wang, K. Pressure Tuning of Optical Properties and Structures in All-Inorganic Halide Perovskite Rb₇Sb₃Cl₁₆. *Inorg. Chem.* **2022**, *61*, 5184–5189. [[CrossRef](#)]
47. Lee, M.; Lee, D.H.D.; Hong, S.V.; Woo, H.Y.; Chae, J.Y.; Lee, D.W.; Han, M.J.; Paik, T. Highly Luminescent and Multifunctional Zero-Dimensional Cesium Lanthanide Chloride (Cs₃LnCl₆) Colloidal Nanocrystals. *Adv. Opt. Mater.* **2022**, *10*, 2102727. [[CrossRef](#)]
48. Park, Y.; Kim, S.H.; Lee, D.; Lee, J.S. Designing Zero-Dimensional Dimer-Type All-Inorganic Perovskites for Ultra-Fast Switching Memory. *Nat. Commun.* **2021**, *12*, 3527. [[CrossRef](#)]
49. Tang, Y.; Liang, M.; Chang, B.; Sun, H.; Zheng, K.; Pullerits, T.; Chi, Q. Lead-Free Double Halide Perovskite Cs₃BiBr₆ with Well-Defined Crystal Structure and High Thermal Stability for Optoelectronics. *J. Mater. Chem. C* **2019**, *7*, 3369–3374. [[CrossRef](#)]
50. Cheng, S.; Nikl, M.; Beitlerova, A.; Kucerkova, R.; Du, X.; Niu, G.; Jia, Y.; Tang, J.; Ren, G.; Wu, Y. Ultrabright and Highly Efficient All-Inorganic Zero-Dimensional Perovskite Scintillators. *Adv. Opt. Mater.* **2021**, *9*, 2100460. [[CrossRef](#)]
51. Seo, J.Y.; Choi, J.; Kim, H.S.; Kim, J.; Yang, J.M.; Cuhadar, C.; Han, J.S.; Kim, S.J.; Lee, D.; Jang, H.W.; et al. Wafer-Scale Reliable Switching Memory Based on 2-Dimensional Layered Organic-Inorganic Halide Perovskite. *Nanoscale* **2017**, *9*, 15278–15285. [[CrossRef](#)]
52. Kim, H.; Choi, M.J.; Suh, J.M.; Han, J.S.; Kim, S.G.; Le, Q.V.; Kim, S.Y.; Jang, H.W. Quasi-2D Halide Perovskites for Resistive Switching Devices with ON/OFF Ratios Above 109. *NPG Asia Mater.* **2020**, *12*, 21. [[CrossRef](#)]
53. Cheng, S.; Beitlerova, A.; Kucerkova, R.; Nikl, M.; Ren, G.; Wu, Y. Zero-Dimensional Cs₃Cu₂I₅ Perovskite Single Crystal as Sensitive X-Ray and γ-Ray Scintillator. *Phys. Status Solidi RRL* **2020**, *14*, 2000374. [[CrossRef](#)]

Disclaimer/Publisher’s Note: The statements, opinions and data contained in all publications are solely those of the individual author(s) and contributor(s) and not of MDPI and/or the editor(s). MDPI and/or the editor(s) disclaim responsibility for any injury to people or property resulting from any ideas, methods, instructions or products referred to in the content.